IJFANS INTERNATIONAL JOURNAL OF FOOD AND NUTRITIONAL SCIENCES
ISSN PRINT 2319 1775 Online 2320 7876
 UGC CARE Listed (Group -I) Journal Volume 11, Iss 11, 2022

Novel SVPWM Using Euclidean Distance Mapping Algorithm For Multilevel Inverters

Dinesh S. Wankhede[1], Mohan V. Aware[2]

[1]Electrical Engineering Department, St. Vincent Pallotti College of Engineering & Technology, Nagpur, Maharashtra, India
[2]Electrical Engineering Department, Visvesvaraya National Institute of Technology, Nagpur, Maharashtra, India

Corresponding author: Dinesh S. Wankhede (e-mail: dineshhwankhede@gmail.com).

ABSTRACT This manuscript presents a novel algorithm for Space Vector Pulse Width Modulated (SVPWM) multilevel inverters (MLI) named as Euclidean distance mapping (EDM). The space vector diagram (SVD) of voltage source inverters (VSI) is processed as an image by the EDM-SVPWM technique; which allows us simplified execution of SVPWM for MLI by doing away with sector recognition, sector based complex trigonometric calculations, extra coordinate transformations and the level based dwell times calculations. An unique switching sequence design algorithm is evolved from the EDM technique, by which improvement in the inverter performance with reference to the factors like stator flux ripple over a sub-cycle, total harmonics distortion (THD) of line voltage, line current ripple and distortion factor (DF) is attained. The EDM-SVPWM technique is validated by analytical treatment and experimentation on hardware prototype.

INDEX TERMS EDM, SVPWM, VSI, MLI, THD, DF, NTV, SVD, Switching Sequence Design, Stator Flux Ripple.

I. INTRODUCTION

Space Vector Pulse Width Modulation (SVPWM) technique gives Vector approach to PWM for 3-phase inverters [1]. SVPWM techniques for Voltage source Inverter (VSI) have been researched rigorously with a variety of objectives like improving DC bus utilisation [1], mitigating line current ripple [2–4], reducing switching loss [7,8] and reduction in torque pulsation [9-11], mitigation in device switching frequency [13] and scope for switching sequence development for enhanced performance [26,27].

The number of switching vectors i.e. voltage vectors of VSI increases with number of levels as it is popular fact that switching vectors are equal to cube of number of levels [1]. SVPWM implementation mainly includes recognition of Nearest Three Voltage-Vectors (NTV), their dwell time calculations and switching sequence development using NTVs. Switching sequence development influence complexity in implementation, harmonic contents in the output of inverter and switching loss.

For MLI execution of SVPWM algorithm becomes complicated affair with increase in number of levels. Many researchers come up with different approaches for SVPWM execution for MLIs with major focus on of NTVs [14-23].

This manuscript presents a novel EDM technique of SVPWM for MLIs. It is simplified, fast and efficient as compared to other SVPWM algorithms as it's execution is free from sector and region recognition, look up tables, sector based complex trigonometric functions, and novel switching sequence design.

In this work the proposed concept of EDM-SVPWM is comprehensively discussed mainly for 2-level and 3-level 3-phase VSIs. Section II gives basics of classical SVPWM. Section III introduces the proposed EDM-SVPWM method for VSIs. In Section IV extension of proposed EDM-SVPWM technique to 3-level 3-phase inverter is discussed briefly. In Section V inverter performance analysis is presented in context of switching sequence designs, stator flux ripple and DF on the basis of analytical treatment. Validations of results of analytical treatment and experimentation on prototype are given in section VI. Section VI also briefly discusses simulation results. Conclusion drawn from this research work are presented in Section VII.

II. CLASSICAL SVPWM FOR TWO-LEVEL VSI

A 2-level VSI is shown in Fig. 1(a) and its SVD in shown in Fig. 1(b). The VSI can switch in 8 possible manners to produce voltage space vectors.

The representation of rotating reference voltage vector, 'V_{ref}' as well as all the switching state vectors for given sampling time is accomplished by use of the d-q transformation in a complex plane.

$$V_{ref} = \begin{bmatrix} V_d \\ V_q \end{bmatrix} = \frac{2}{3} \begin{bmatrix} 1 & cos(\frac{2\pi}{3}) & cos\left(\frac{2\pi}{3}\right) \\ 0 & sin(\frac{2\pi}{3}) & -sin\left(\frac{2\pi}{3}\right) \end{bmatrix} \begin{bmatrix} V_a \\ V_b \\ V_c \end{bmatrix} \quad (1)$$

Where,

ISSN PRINT 2319 1775 Online 2320 7876
 UGC CARE Listed (Group -I) Journal Volume 11, Iss 11, 2022

V_a, V_b & V_c represent the phase voltages for balanced three phase system and
V_d & V_q represent d-axis and q-axis component of the V_{ref}.
A sampled V_{ref}, as shown in Fig. 1(b) is synthesized by maintaining volts-second balance among the NTVs and is formulated by the following equation

$$V_{ref} T_s = V_1 \frac{T_1}{T_s} + V_2 \frac{T_2}{T_s} + V_0 \frac{T_0}{T_s} \quad (2)$$

$$V_{ref} = V_1 T_1 + V_2 T_2 + V_0 T_0 \quad (3)$$

$$T_s = T_1 + T_2 + T_0 \quad (4)$$

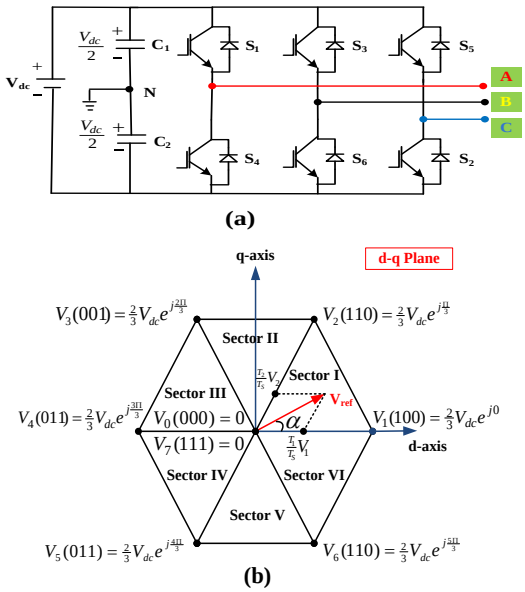

FIGURE 1 (a) Power Circuit of 2- Level VSI
FIGURE 1 (b) The decomposition of V_{ref} at sector 1 in SVD of 2-level VSI.

Where,
T_1, T_2 & T_0 represent the 'ON' time durations for NTVs V_1, V_2 & V_0 respectively.

$$T_s = \frac{1}{f_s} \quad (5)$$

T_s = Time duration of switching needed; and
f_s = Frequency of Switching.

'ON' time durations for $0° \leq \alpha \leq 360°$

$$T_1 = \frac{\sqrt{3}.T_s.|\bar{V}_{ref}|}{V_{dc}} \left(\sin\frac{n\pi}{3}\cos\alpha - \cos\frac{n\pi}{3}\sin\alpha \right) \quad (6)$$

$$T_2 = \frac{\sqrt{3}.T_s.|\bar{V}_{ref}|}{V_{dc}} \left(\sin\alpha\cos\frac{(n-1)\pi}{3} - \cos\alpha\ \sin\frac{(n-1)\pi}{3} \right) \quad (7)$$

Where,
α = angle between the V_{ref} and the direct axis.

The SVPWM realization in classical way requires sector recognition in which the V_{ref} is located, identification of the 'NTV's, computing their respective "Dwell' times and suitable switching sequence design for each sample time.

III. PROPOSED TECHNIQUE OF SVPWM EXECUTION USING EDM

The realization of EDM-SVPWM for VSI can be accomplished by performing following steps.

A. DETERMINATION OF X-Y COORDINATES OF V_{REF}

By applying following steps mapping of x-y coordinates of V_{ref} can be accomplished.

1) STEP 1

Select the switching frequency (f_s) and M. I. for which the VSI is to be operated.

2) STEP 2

Compute the magnitude of the V_{ref} from V_{dc} and M. I. by using equation (8).

$$M.I. = \frac{\sqrt{3}V_{ref}}{V_{dc}} \quad (8)$$

3) STEP 3

Compute the coordinates of V_{ref} by using equation (9) and (10).

$$V_{dr} = |V_{ref}| \cos\alpha \quad (9)$$

$$V_{qr} = |V_{ref}| \sin\alpha \quad (10)$$

where,
V_{dr} = direct axis coordinate of V_{ref};
V_{qr} = quadrature axis coordinate of V_{ref};
α = angle between the V_{ref} and the direct axis.

4) STEP 4

The above mentioned steps 1, 2 and 3 are repeated for 'P' times in one cycle and repeated continuously later on.

$$P = \frac{\frac{1}{f_1}}{\frac{1}{f_s}}. \quad (11)$$

$$\delta = \frac{360}{P} \quad (12)$$

$$f_s = \frac{1}{T_s} \quad (13)$$

$$\alpha_{(j+1)} = Initail\ angle\ \alpha + \delta \quad (14)$$

where,
P = total sampling points in one cycle i.e. 360°,
δ = angle of rotation of V_{ref},
f_1 = fundamental frequency;

ISSN PRINT 2319 1775 Online 2320 7876
 UGC CARE Listed (Group -I) Journal Volume 11, Iss 11, 2022

f_s = switching frequency;
T_s = sampling time,
j = 1, 2, ...P.

B. DETERMINATION OF X-Y COORDINATES OF ALL SWITCHING VECTORS

The angles and magnitudes of all 8 switching vectors are shown in Fig. 1 (b). Their x-y axis coordinates are obtained accordingly and can be stored in arrays $X_{v[i]}$ & $Y_{v[i]}$ as shown in equation (17). For two-level VSI there will be seven locations of eight switching vectors or stationary vectors as there is one redundant vector at the centre of SVD.

C. DETERMINATION OF NTV BY EDM

The ED between tip of V_{ref} and all eight switching vectors as shown in Fig. 2(a) are calculated and stored in an array $D_{[i]}$

$$D_{[i]} = \sqrt{\left(X_{ref} - X_{v[i]}\right)^2 + \left(Y_{ref} - Y_{v[i]}\right)^2} \qquad (15)$$

where,
D = the ED between V_{ref} and any switching state; i = 0, 1, 2, ... (n^3- 1) (n = number of levels of MLI); X_{ref} = X-axis coordinate of reference vector;
Y_{ref} = Y-axis coordinate of reference vector;
X_v = X-axis coordinate of stationary vector;
Y_v = Y-axis coordinate of stationary vector.

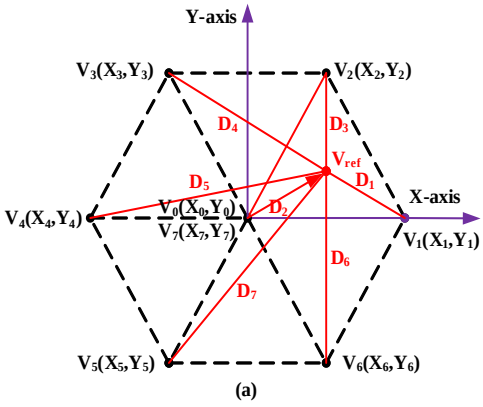

FIGURE 2 (a) EDs between V_{ref} and all eight switching vectors in X-Y plane for two-Level SVPWM Voltage Source Inverter

The NTVs from V_{ref} for a particular sampling point are obtained by simply sorting out the EDs of all switching vectors in ascending order. Let D_1, D_2 & D_3 be the EDs of first nearest vector (FNV), second nearest vector (SNV) and third nearest vector (TNV) respectively.

D. DWELL TIME CALCULATIONS

The dwell times of NTV of the V_{ref} as shown in Fig. 2 (a) in any position in SVD of VSI can be found by using following equations represented in matrix form [24],[25].

$$\begin{bmatrix} T_1 \\ T_2 \\ T_3 \end{bmatrix} = \begin{bmatrix} V_{d1} & V_{d2} & V_{d3} \\ V_{q1} & V_{q2} & V_{q3} \\ 1 & 1 & 1 \end{bmatrix}^{-1} \begin{bmatrix} V_{dr} \\ V_{qr} \\ 1 \end{bmatrix} T_s \qquad (16)$$

where,
T_1, T_2 & T_3 represent the "Dwell Times" of the NTV;
V_{d1}, V_{d2} & V_{d3} are direct axis or X-axis coordinates of NTV;
V_{q1}, V_{q2} & V_{q3} are quadrature axis or Y-axis coordinates of NTV;
V_{dr} is direct axis or X-axis coordinate of reference vector V_{ref} and
V_{qr} is quadrature axis or Y-axis coordinate of reference vector V_{ref}.

NTV are treated in ascending order of EDs from V_{ref}. Refer Fig. 2 (b) which shows only V_{dr} ,V_{qr}, V_{d3} & V_{q3} for the sake of simplicity.

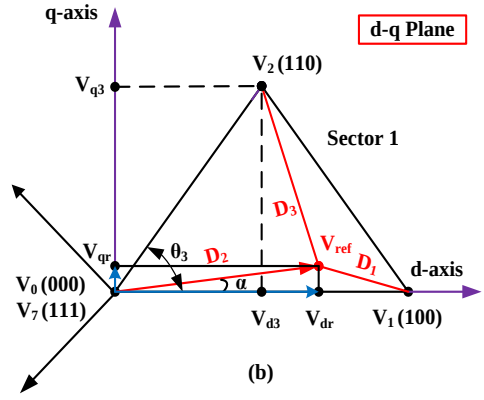

FIGURE 2 (b) Reference voltage vector V_{ref} and its component in d-q axis.

The direct axis or X-axis coordinate of switching vector is defined by,

$$V_d^* = |V| cos\theta_* \qquad (17)$$

The quadrature axis or Y-axis coordinate of switching vector is defined by,

$$V_q^* = |V| sin\theta_* \qquad (18)$$

where, θ = Angle between the *d*-axis and stationary switching vector among NTV and
* = 1 or 2 or 3 (i.e. order of NTV).
The direct axis or X-axis coordinate of V_{ref} i.e. V_{dr} and the quadrature axis or Y-axis coordinate of V_{qr} can be found by referring "(9)" and "(10)".

E. DEVELOPEMENT OF SWITCHING SEQUENCE

ISSN PRINT 2319 1775 Online 2320 7876
 UGC CARE Listed (Group -I) Journal Volume 11, Iss 11, 2022

THD of the output current and voltage depends on design of switching sequence [4], [29]. For the location of V_{ref} shown in Fig. 3 (a) the FNV = V_1; the SNV = V_0; and the TNV = V_2. For the location of V_{ref} shown in Fig. 3 (b) the FNV = V_2; the SNV = V_1 and the TNV = V_0. In EDM-SVPWM, the FNV for time 'T_1'is applied first, the SNV for time 'T_2' is applied after FNV and at last the TNV for time 'T_3' is applied.

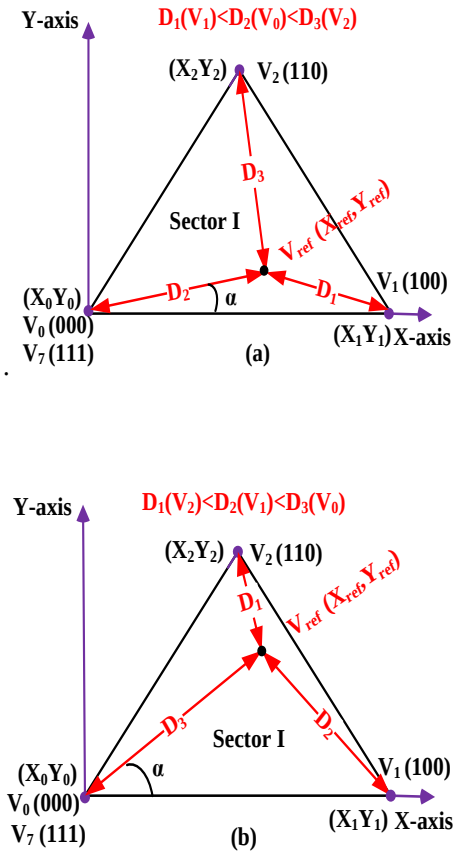

FIGURE 3. Sequence of NTV on the basis of EDM **(a)** Case 1 **(b)** Case 2

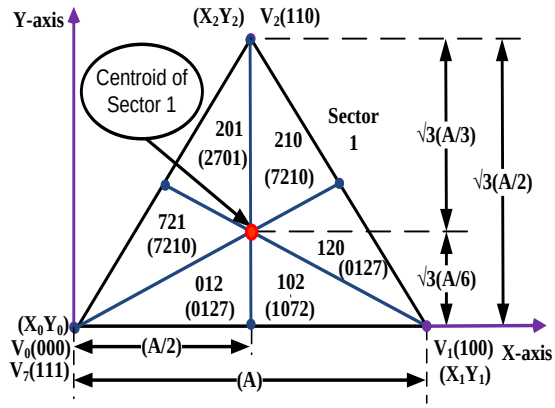

FIGURE 4. The 6-zones created by EDM for sector I of SVD of two level SVPWM inverter.

Each sector of SVD gets divided in 6 zones on the basis of EDs of NTVs from the V_{ref}. To maintain symmetry and to avoid DC offset in output voltage zero and redundant switching states are duly applied. Fig. 4 shows these 6-zones in reference of first sector. The EDM-SVPWM algorithm for *n* - level 3-phase VSI is given in Fig. 5.

IV. EXTENSION OF PROPOSED EDM-SVPWM TECHNIQUE TO 3-PHASE 3-LEVEL VSI

The EDM-SVPWM technique is basically aimed to simplify execution of SVPWM for MLI in general but with higher number of levels in specific such as the "Trans Bay Cable Project", in which 216 voltage-levels are reported to have achieved [32]. For implementation of EDM-SVPWM to MLI with any arbitrary value of number of levels in MLI i.e. $'n' > 2$, some corrections are needed exclusively in the subsection B of the section III, as it is dynamic to the *'n'* and looks after creation of SVD, which is very much important for the EDM-SVPWM method. The SVD becomes complicated with increasing the value of *'n'* . SVD creation is accomplished by a computer program, Fig. 5, shows it's flow chart.

ISSN PRINT 2319 1775 Online 2320 7876
 UGC CARE Listed (Group -I) Journal Volume 11, Iss 11, 2022

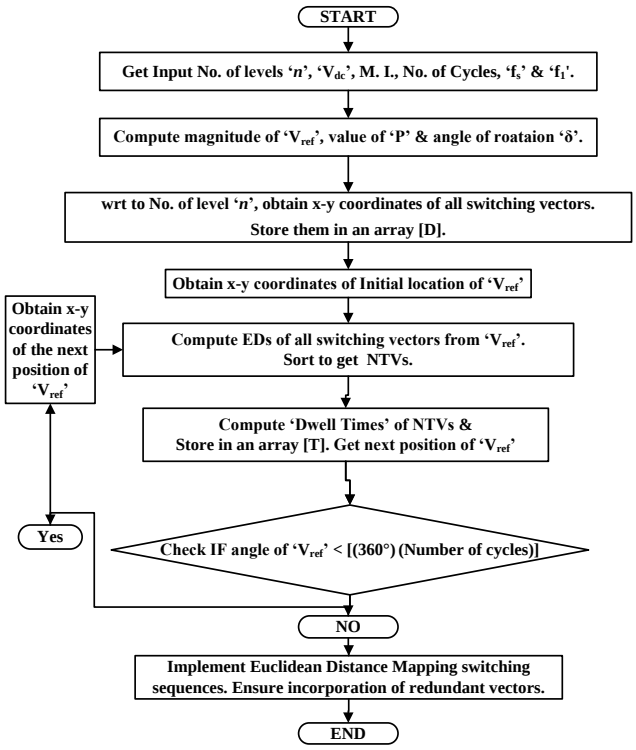

FIGURE 5. EDM-SVPWM algorithm for *n*-level 3-phase MLI

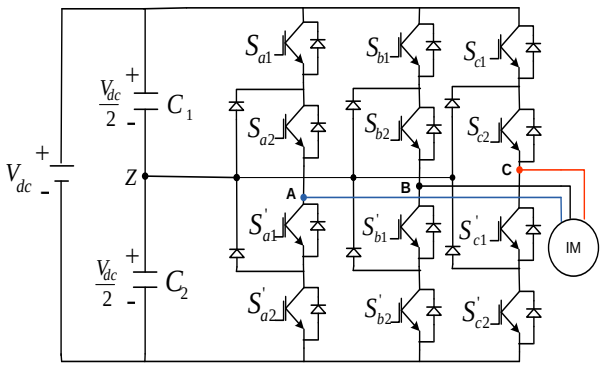

FIGURE 6 a. Three level SVPWM inverter (NPC) circuit diagram.

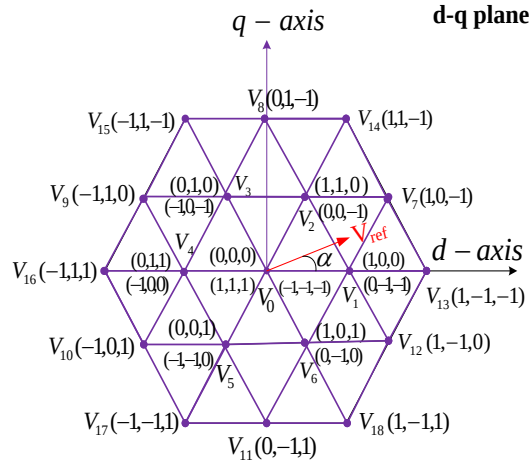

FIGURE 6 b. SVD of three-level SVPWM inverter

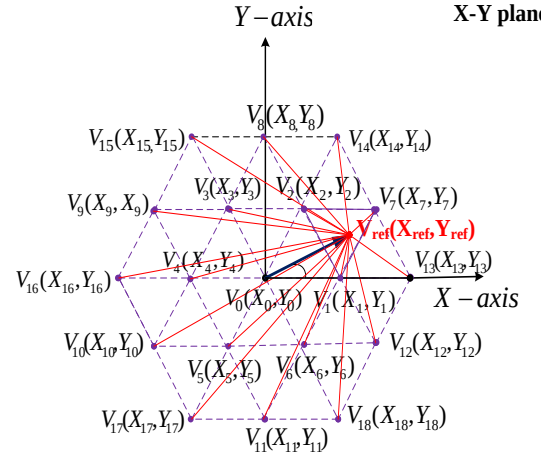

FIGURE 6 c. V_{ref} and its EDs between all 27 switching vectors X-Y plane for three-level SVPWM inverter.

Consider the neutral point clamped (NPC) 3-level VSI *(n=3)* shown in Fig. 6a and its SVD is shown in Fig. 6b. There are $3^3 = 27$ possible switching vectors, located at 19 positions. Fig. 6c shows, all switching states and their EDs from the V_{ref} highlighted in red colour. The ED calculations of x-y co-ordinates of stationary switching vectors, which determined by *'n'* of MLI and x-y co-ordinates of V_{ref} holds key for EDM techniques execution.

V. VSI PERFORMANCE ANALYSIS

A. SWITCHING SEQUENCE DESIGNS

In conventional sequence 0127, as shown in Fig. 7(a), all 3-phases switch once in a subcycle. case of 'Double-switching clamping (DSC) sequences, in each subcycle, one phase switches twice, another switches once, and the third phase is clamped. DSC sequences are proposed and investigated recently for a two-level inverter [29], [31]. These are shown in Fig. 7 (b)–(e). For the given average switching frequency and MI almost equal to 1.0, the DSC sequences 7212 and 0121 effects mitigation in THD value

ISSN PRINT 2319 1775 Online 2320 7876
 UGC CARE Listed (Group -I) Journal Volume 11, Iss 11, 2022

of line current. The DSC Sequences 1012 and 2721 achieve reduction the torque ripple in motor drives [9]-[11]. Mitigation of switching loss is obtained with proper combination of DSC sequences in 2-level inverters [7]. This manuscript presents EDM switching sequence and their performances are compared with conventional and DSC sequences.

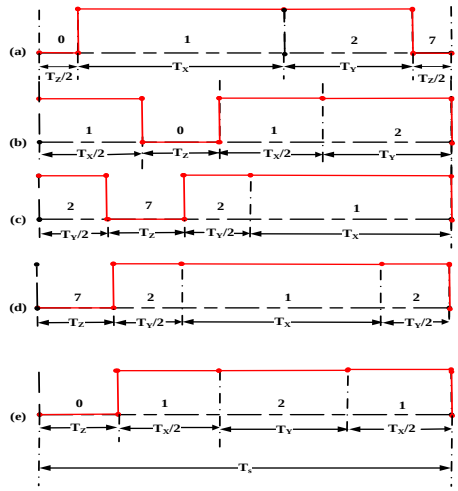

FIGURE 7. Double-switching clamping sequences for two-level inverter **(a)** 0127 **(b)** 1012 **(c)** 2721 **(d)** 7212 **(e)** 0121

All redundant vectors in any SVD produce same ripple [28]. Following are the probable sequences applicable in VSI; (i) 012 (ii) 021 (iii) 102 (iv) 120 (v) 201 (vi) 210. Refer Fig. 8. But it is found that the pattern of mean square ripple 'F_{SEQ}^2' with reference to angle α° for a sector for the sequence 012 is the same for the sequence 210. The sequences 021 & 120 as well as 102 & 201 repeats similar story. Hence rather than considering above mentioned 6 probable sequences only 3 sequences are considered for analysis which are 012, 102 and 021.

In the same manner, it is observed that the for sequence 123 and 321 gives exactly same pattern of mean square ripple 'F_{SEQ}^2' at angle α° for a given sector. Refer Fig. 9. The sequences 132 & 231 as well as the sequences 213 & 312 gives same result.

Hence following sequences are considered for performance investigations (i) 012, (ii) 021, (iii) 102, (iv) 123, (v) 132, (vi) 213, (vii) 7212, (viii) 0121, (ix) 2721, (x) 1012 and (xi) 0127.

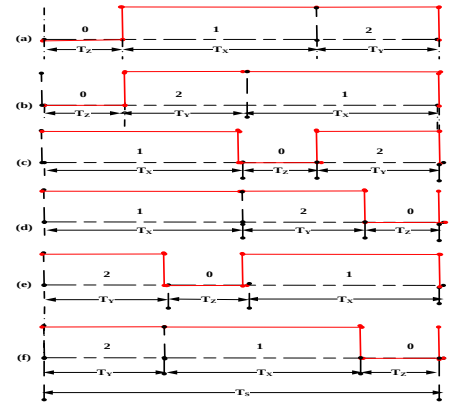

FIGURE 8. Switching sequences for two-level inverter **(a)** 012 **(b)** 021 **(c)** 102 **(d)** 120 **(e)** 201 **(f)** 210

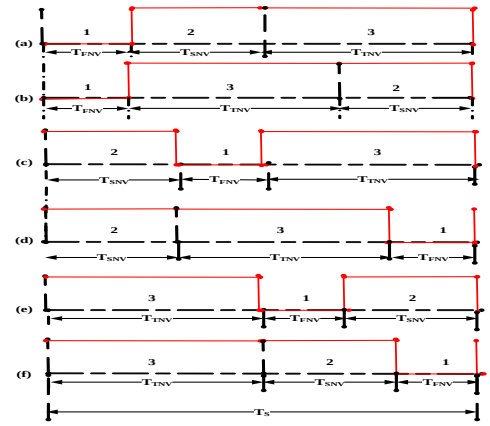

FIGURE 9. EDM sequences for two-level inverter **(a)** 123 **(b)** 132 **(c)** 213 **(d)** 231 **(e)** 312 **(f)** 321

B. ANALYTICAL TREATMENT WITH REFERENCE TO THE STATOR FLUX RIPPLE

In case of PWM inverter fed IM drive, the ripple in line current is created due to the instantaneous error between the V_{ref} and the applied voltage [1], [2], [10], [28]. The error voltage vectors of NTVs V_1, V_2 and V_7 respectively are shown in Fig. 8 for V_{ref} = 0.4 $V_{dc}\angle 15°$. The error voltage vectors can be formulated as given below;

$$V_{err1} = V_1 - V_{ref} \quad (19)$$

$$V_{err2} = V_2 - V_{ref} \quad (20)$$

$$V_{err0} = V_0 - V_{ref} \quad (21)$$

The "Stator Flux Ripple Vector" can be defined as the time integral of the error voltage vector, which is measure of current ripple in motor [28]. For sequence 0127, as shown in Fig. 8, the triangular shaped trajectory of the tip of the "Stator Flux Ripple Vector (Ψ)" is created. The "Stator Flux Ripple Vector (Ψ)" can be resolved along *d* & *q* axis. The *q*-axis coincides with the 'V_{ref}' as shown in Fig. 8. The sides of the triangular trajectory are equal to $V_{err1}T_1$, $V_{err2}T_2$ and $V_{err}T_Z$ and correspond to the NTVs (V_1, V_2 and V_7 or V_0). The q axis components of the three sides are Q_1, Q_2 and Q_Z, respectively, as defined as given below;

ISSN PRINT 2319 1775 Online 2320 7876
 UGC CARE Listed (Group -I) Journal Volume 11, Iss 11, 2022

$$Q_1 = [V_{dc}\cos(\alpha) - V_\alpha]T_1 \quad (22)$$

$$Q_2 = [V_{dc}\cos(60^\circ - \alpha) - V_\alpha]T_2 \quad (23)$$

$$Q_Z = -V_\alpha T_Z. \quad (24)$$

The side $V_{errZ}T_Z$ has no component along the d axis. The projection of the other 2 sides of the triangle on the d axis is given by 'D' defined as given below;

$$D = V_{dc}\sin(\alpha)T_1 = V_{dc}\sin(60^\circ - \alpha)T_2 \quad (25)$$

The d and q-axis components of the flux ripple vector are shown in terms of Q_1, Q_2, Q_Z and D in Fig. 10. In this manuscript the mean square values of ψ_x and ψ_y over the subcycle for the sequence 0127 ($F^2_{x,0127}$ and $F^2_{y,0127}$, respectively) are calculated by using the method presented in [28]. The mean square value of the total stator flux ripple over the subcycle is calculated a follows;

$$F^2_{0127} = F^2_{x,0127} + F^2_{y,0127} \quad (26)$$

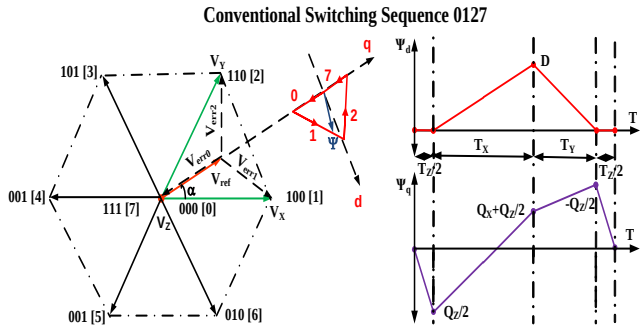

FIGURE 10. Stator Flux Ripple Vector (Ψ) & Error Voltage Vectors corresponding to NTVs i.e. V_1, V_2 and V_7 for Sequence 0127.

TABLE I

F^2_{0127} in Terms of Q_1, Q_2, Q_Z and D, over a Subcycle for Sequence 0127.

Sr. No.	Switching Sequence	Expression for $F^2_{SEQUENCE}$ i. e. Mean Square Ripple
1	0127	$F^2_{0127} = \frac{1}{3Ts}\{[(0.5Q_z^2)T_z)] + [(0.5Q_z^2 + (Q_x + 0.5Q_z)0.5Q_z + (Q_x + 0.5Q_z)^2]T_x + [(Q_x + 0.5Q_z)^2 - (Q_x + 0.5Q_z)Q_z + (-0.5Q_z)^2]T_y + (-0.5Q_z^2)0.5T_z) + [0.5D^2(T_x + T_y)]\}$

ISSN PRINT 2319 1775 Online 2320 7876
 UGC CARE Listed (Group -I) Journal Volume 11, Iss 11, 2022

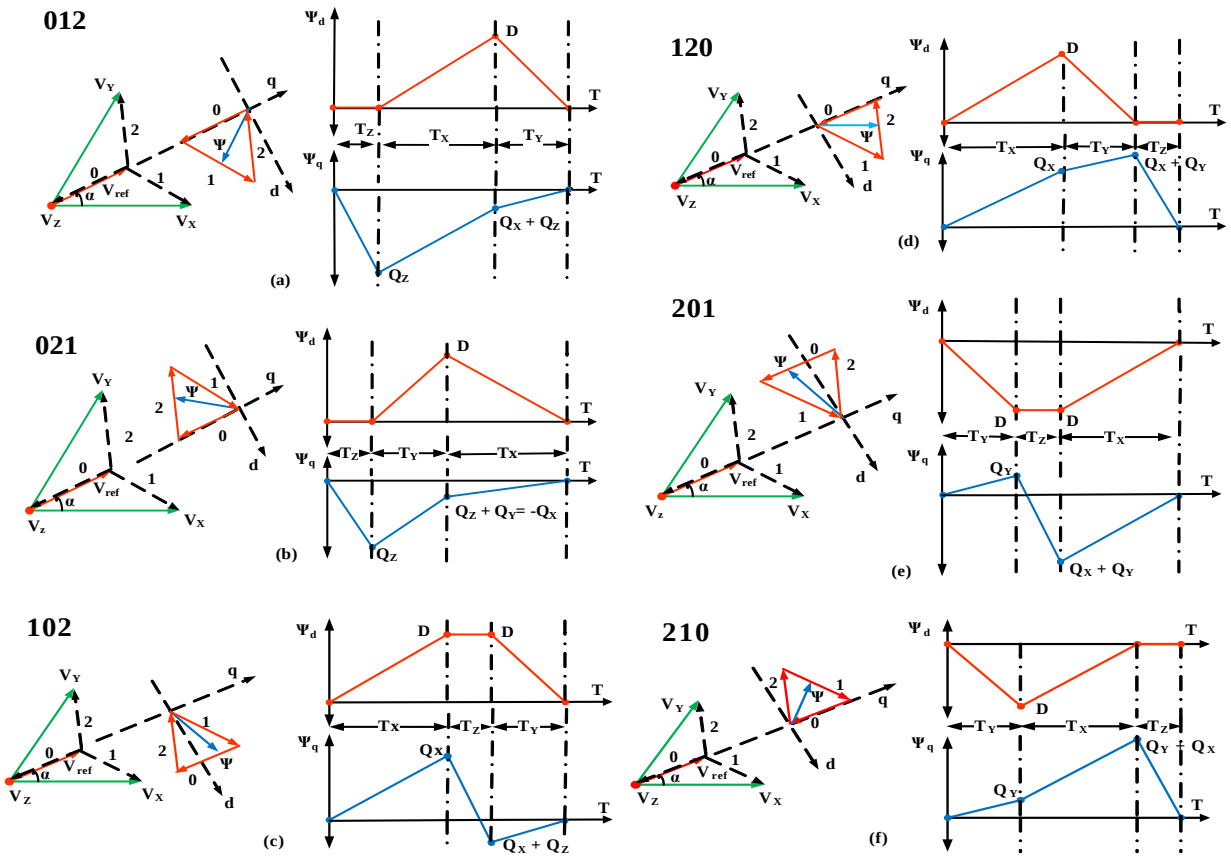

FIGURE 11. Stator Flux Ripple Vector (Ψ) over a Subcycle and it's components along d & q-axis corresponding to the 6 probable sequences **(a)** 012 **(b)** 021 **(c)** 102 **(d)** 120 **(e)** 201 **(f)** 210

TABLE II
$F^2_{SEQUENCE}$ OVER A SUBCYCLE : Q_1, Q_2, Q_Z & D FOR THE 6 PROBABLE SWITCHING SEQUENCES.

Sr. No.	Switching Sequence	Expression for $F^2_{SEQUENCE}$ i. e. Mean Square Ripple
1	012	$F^2_{012} = \frac{1}{3Ts}\{[(Q_z^2)T_z)] + [(Q_z^2 + (Q_x + Q_z)Q_z + (Q_x + Q_z)^2]T_x + [(Q_x + Q_z)^2]T_y + [D^2(T_x + T_y)]\}$
2	021	$F^2_{021} = \frac{1}{3Ts}\{[(Q_z^2 T_z)] + [(Q_z^2 + (Q_z)(-Q_x) + (Q_x)^2]T_y + [(Q_x)^2]T_y + [D^2(T_x + T_y)]\}$
3	102	$F^2_{102} = \frac{1}{3Ts}\{[(Q_x^2)T_x)] + [(Q_x^2 + (Q_x + Q_z)Q_x + (Q_x + Q_z)^2]T_z + [(Q_x + Q_z)^2]T_y + [D^2(T_x + T_y) + 3D^2T_z]\}$
4	120	$F^2_{120} = \frac{1}{3Ts}\{\left[(Q_x^2)T_x)\right] + [(Q_x^2 + (Q_x + Q_y)Q_x + (Q_x + Q_y)^2\right]T_x + \left[(Q_x + Q_y)^2\right]T_z + [D^2(T_x + T_y)]\}$
5	201	$F^2_{201} = \frac{1}{3Ts}\{\left[(Q_y^2)T_y)\right] + [(Q_y^2 + (Q_z + Q_y)Q_y + (Q_z + Q_y)^2\right]T_z + \left[(Q_z + Q_y)^2\right]T_x + [D^2(T_x + T_y) + 3D^2T_z]\}$

ISSN PRINT 2319 1775 Online 2320 7876
 UGC CARE Listed (Group -I) Journal Volume 11, Iss 11, 2022

6	210	$F_{210}^2 = \frac{1}{3Ts}\{[(Q_y^2)T_y)] + [(Q_y^2 + (Q_x + Q_y)Q_y + (Q_x + Q_z)^2]T_x + [(Q_x + Q_z)^2]T_z + [D^2(T_x + T_y)]\}$

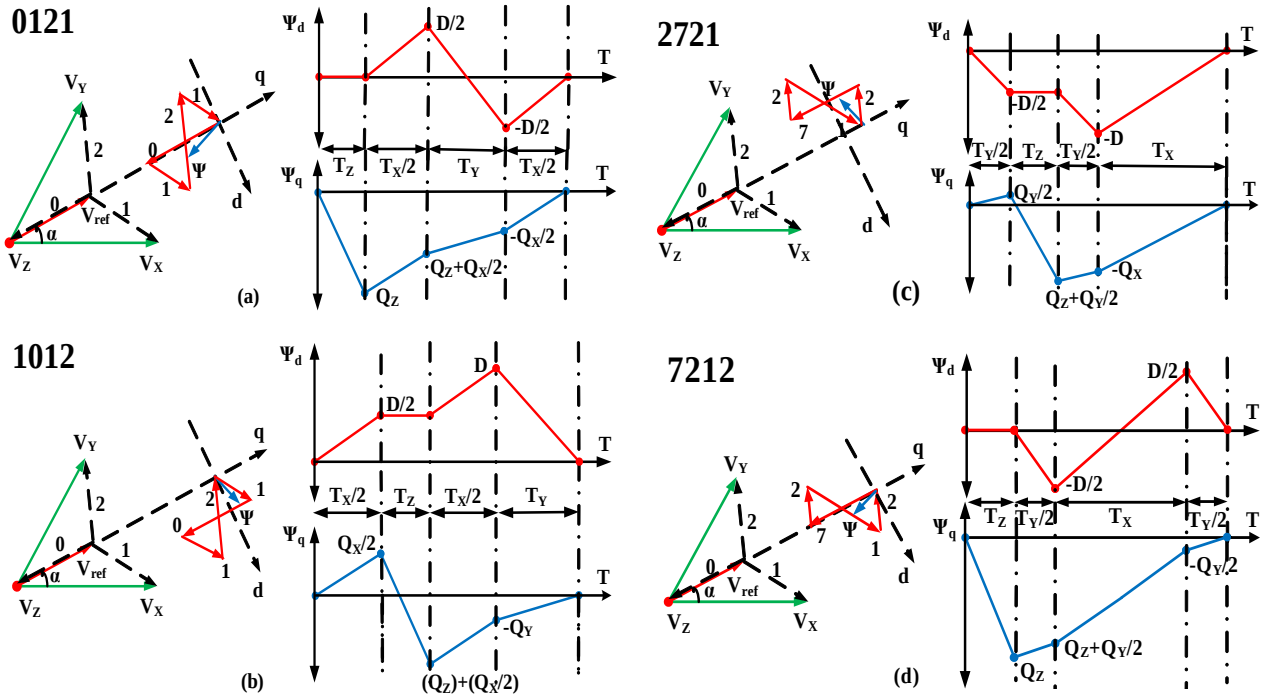

FIGURE 12. Stator Flux Ripple Vector (Ψ) over a subcycle and its components along d & q-axis corresponding to the DSC sequences **(a)** 0121 **(b)** 2721 **(c)** 102 **(d)** 7212

TABLE III
$F_{SEQUENCE}^2$ OVER A SUBCYCLE IN TERMS OF Q_1, Q_2, Q_Z AND D FOR THE DSC SEQUENCES.

ISSN PRINT 2319 1775 Online 2320 7876
Research paper UGC CARE Listed (Group -I) Journal Volume 11, Iss 11, 2022

Sr. No.	Switching Sequence	Expression for $F^2_{SEQUENCE}$ i. e. Mean Square Ripple
1	0121	$F^2_{0121} = \frac{1}{3Ts}\{[(Q_z^2)T_z)] + [(Q_z^2 + (0.5Q_x + Q_z)Q_z + (0.5Q_x + Q_z)^2]T_x + [(0.5Q_x + Q_z)^2 - (0.5Q_x + Q_z)0.5Q_x + (-0.5Q_x)^2]T_y + (0.5Q_x^2)0.5T_x) + [0.5D^2(T_x + T_y)]\}$
2	1012	$F^2_{1012} = \frac{1}{3Ts}\{[(0.5Q_x^2)0.5T_x)] + [(0.5Q_x^2 + (0.5Q_x + Q_z)0.5Q_x + (0.5Q_x + Q_z)^2]T_Z + [(0.5Q_x + Q_z)^2 - (Q_x + Q_z)(0.5Q_X + Q_z) + (Q_x + Q_z)^2]0.5T_X + (Q_x + Q_z)^2T_Y + [D^2(T_x + T_Y + \frac{3}{4}T_Z)]\}$
3	2721	$F^2_{2721} = \frac{1}{3Ts}\{[(0.5Q_Y^2)0.5T_Y)] + [(0.5Q_Y^2 + (0.5Q_Y + Q_Z)0.5Q_Y + (0.5Q_Y + Q_Z)^2]T_Z + [(-Q_X)^2 - (Q_x)(0.5Q_Y + Q_Z) + (0.5Q_Y + Q_Z)^2]0.5T_Y + (Q_X)^2T_X + [D^2(T_x + T_Y + \frac{3}{4}T_Z)]\}$
4	7212	$F^2_{7212} = \frac{1}{3Ts}\{\left[(Q_z^2)T_z)\right] + [(Q_z^2 + \left(0.5Q_y + Q_z\right)Q_z + \left(0.5Q_y + Q_z\right)^2\Big]T_y + \Big[\left(0.5Q_y + Q_z\right)^2 - \left(0.5Q_y + Q_z\right)0.5Q_y + (-0.5Q_y)^2\Big]T_x + \left(0.5Q_y^2\right)0.5T_y) + [0.5D^2(T_x + T_y)]\}$

ISSN PRINT 2319 1775 Online 2320 7876
 UGC CARE Listed (Group -I) Journal Volume 11, Iss 11, 2022

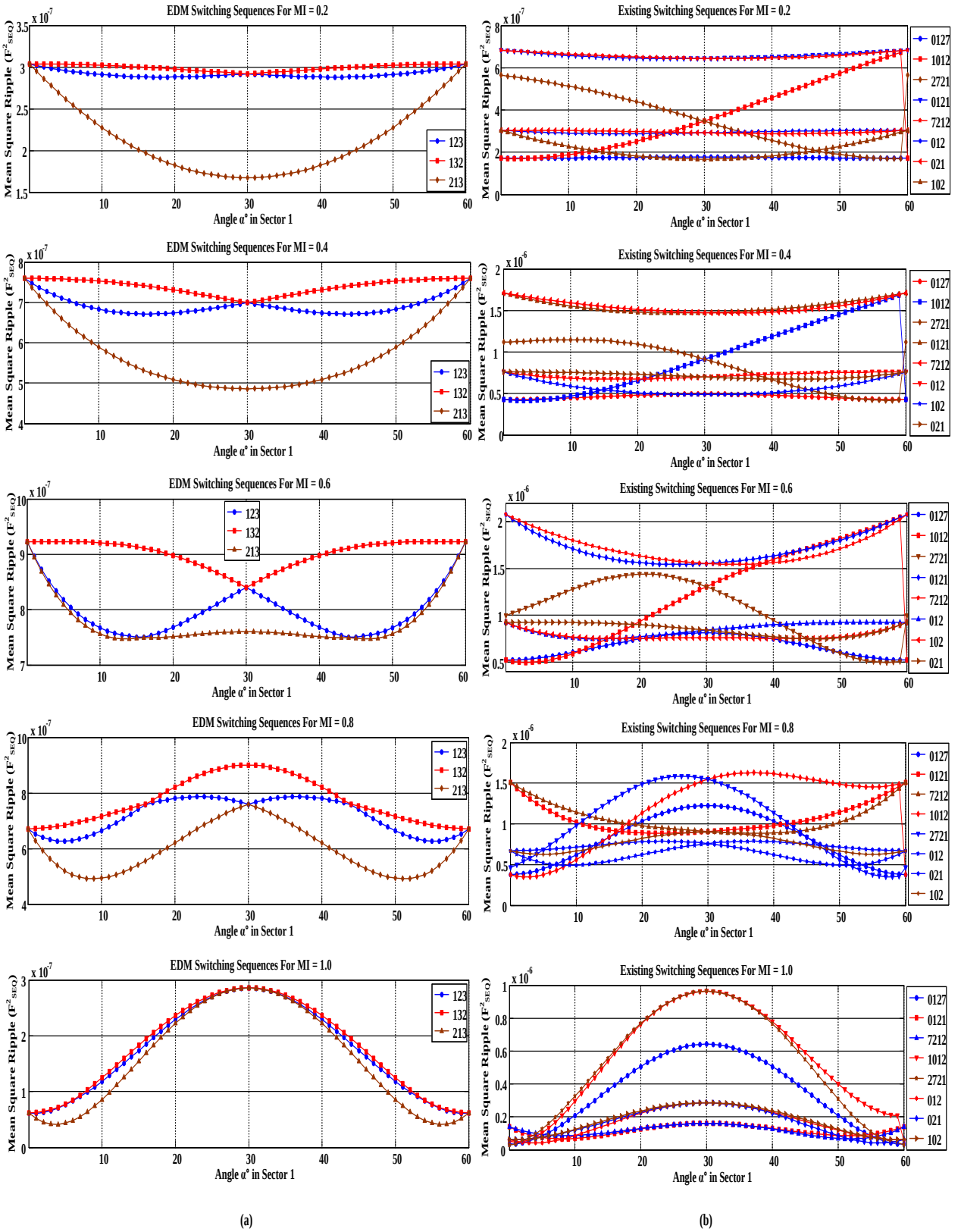

FIGURE 13. Comparison of $F^2_{SEQUENCE}$ for 0° ≤ α ≤ 60° for MI = 0.2, 0.4, 0.6, 0.8, 1.0.

(a). For EDM-SVPWM sequences123, 213 & 132 (b). For sequences 012, 021, 102, 0127, 1012, 0121, 7212 and 2721

The expression for F^2_{0127} is presented in the Table I. The expressions for F^2_{012}, F^2_{021}, F^2_{102}, F^2_{120}, F^2_{201} and F^2_{210} are obtained from Fig. 11 (a)–(f), respectively and presented in Table II. The expressions for F^2_{0121}, F^2_{1012}, F^2_{2721} and F^2_{7212} can also be obtained at from Fig. 12 (a)–(d), respectively. These expressions are presented in Table III.

C. RESULTS AND DISCUSSIONS : STATOR FLUX RIPPLE

Fig. 13 (a) and (b) presents 'F^2_{SEQ}' for the first sector 1 for MIs values raging from 0 to 1.0, for 'EDM' sequences 123, 213 and 132 and for switching sequences 012, 021, 102, 0127, 1012, 0121, 7212 and 2721 respectively. Results presented in Fig. 13 (a) and (b) proves that with reference to 'F^2_{SEQ}', the EDM sequence are far better than all other prominent switching sequences. Among the EDM sequences, the sequence 231 obtains the best results.

D. ANALYTICAL TREATMENT USING THE DISTORTION FACTOR

The F_{DIST} i.e. total root mean square (RMS) harmonic DF based on stator flux ripple is acquired by normalizing the RMS value of ripple in stator flux over a sector with reference to the fundamental flux (ψ_1) as given below;

$$F_{DIST} = \frac{1}{\psi_1}\sqrt{\frac{3}{\pi}\int_0^{\frac{\pi}{3}} F_{SEQ}^2 d\alpha} = \sqrt{\sum_{SECTOR} \frac{F_{SEQ}^2}{N\psi_1^2}} \qquad (27)$$

$$\psi_1 = \frac{V_{ref}}{2\pi f_1} = \frac{3NT_sV_{ref}}{\pi} \qquad (28)$$

where,
N = Number of samples per sector.

The RMS value of total ripple in line current is obtained by using the analytical evaluation of the DF 'F_{DIST}'. The DF 'F_{DIST}' does not depends on machine parameters [28].

E. RESULT AND DISCUSSIONS : DISTORTION FACTOR

Fig. 14 (a) and (b) shows comparison of performance of EDM switching sequences with other prominent switching sequences with reference to MIs and DF F_{DIST}.

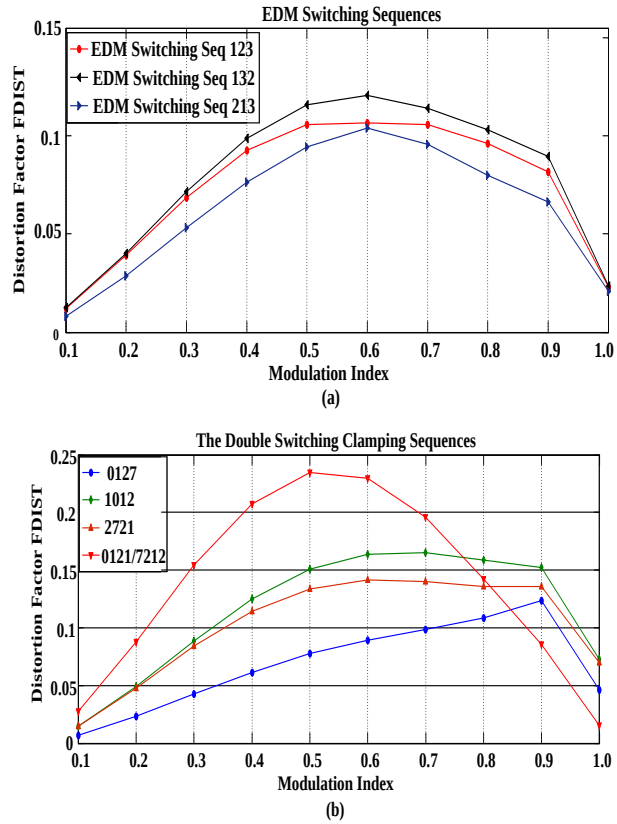

FIGURE 14. (a) DF F_{DIST} corresponding to EDM switching sequences 123, 213and 132 at Unity MI.
(b) DF F_{DIST} corresponding to switching sequences 0127, 0121, 1012, 7212, 2721 at Unity MI.

For all MIs among the three EDM switching sequences, the lowest F_{DIST} is given by the sequence 213, the highest F_{DIST} is given by the sequence 132 and the sequence 123 gives the moderate F_{DIST}. All EDM switching sequences achieves low value of F_{DIST} as compared to DSC sequences. DSC sequences gives exactly same F_{DIST} and their F_{DIST} is highest for MIs from 0.1 to 0.7 and lowest for MI 0.9 and 1.0. Conventional sequence 0127 performs exactly reverse to the DSC Sequence 7212 and 0121 i.e. it gives lowest F_{DIST} for MIs from 0.1 to 0.7 and for MIs 0.8 to 1.0 F_{DIST} given is higher than EDM switching sequences and DSC Sequences 7212 and 0121. F_{DIST} of DSC sequence 1012 is only better than 7212/0121 for lower MIs from 01. to 0.7 and highest for MI 0.9 and 1.0. Overall for all spread of MIs, the EDM switching sequence 213 performs better through the spread of MIs.

As far as F_{DIST} is concerned, the EDM- SVPWM method yeilds 7.4% , 54.3%, 44.7%, 38.2%, average reduction as compared with switching sequences 0127, 0121, 1012 and 2721 respectively.

% reduction in distortion factor 'F_{DIST}' with EDM 213 as compared to any other switching sequence 'X' are calculated as follows

ISSN PRINT 2319 1775 Online 2320 7876
 UGC CARE Listed (Group -I) Journal Volume 11, Iss 11, 2022

$$\text{Average \% reduction in '}F_{DIST}\text{' with EDM 213} = \left(\frac{\Sigma F_{DIST}\ For\ Sequence\ X - \Sigma F_{DIST}\ For\ EDM\ 213}{\Sigma F_{DIST}\ For\ Sequence\ X}\right) * 100 \quad (27)$$

Results shown in Fig. 14a. for 'F_{DIST}' are presented in tabulated form in Table IV along with average % reduction values of other switching sequences.

TABLE IV
OBSERVATIONS FOR AVERAGE % REDUCTION IN THE DF 'F_{DIST}' FOR EDM-SVPWM METHOD AS COMPARED TO OTHER PROMINENT SEQUENCES.

Sr. No.	M. I.	% Current THD				
		EDM	Switching Sequence			
		213	0127	1012	2721	0121
1	0.1	0.01	0.01	0.01	0.02	0.03
2	0.2	0.03	0.02	0.05	0.05	0.09
3	0.3	0.05	0.04	0.09	0.08	0.15
4	0.4	0.08	0.06	0.12	0.11	0.21
5	0.5	0.09	0.08	0.15	0.13	0.23
6	0.6	0.10	0.09	0.16	0.14	0.23
7	0.7	0.10	0.10	0.16	0.14	0.20
8	0.8	0.08	0.11	0.16	0.14	0.14
9	0.9	0.07	0.12	0.15	0.14	0.09
10	1.0	0.02	0.05	0.07	0.07	0.02
Total (Σ)		**0.63**	**0.68**	**1.14**	**1.02**	**1.38**
Average % Reduction			**7.35**	**44.73**	**38.23**	**54.34**

VI. EXPERIMENTATION ON HARDWARE PROTOTYPE FOR VALIDATION

The 'EDM-SVPWM' method is verified by experimentation on prototype built in laboratory of 3-phase VSI for various MIs and fundamental frequencies. The experimentation done with V_{dc} = 150 V, f_s = 2.44 kHz, T_s = 0.4098 ms, 50 Hz, 45Hz, 40Hz, 35Hz and 30Hz are the fundamental frequencies, C_1= C_2=1000 µF and 200 V. 3-phase, 415 V, 2 kW, R-L load is connected to the VSI and insulated gate bipolar transistor (IGBT) (FGA25N120ANTD) operated with dead time = 1 µs are used as switches. KBPC3510 used as 1-phase diode bridge rectifier, gives input DC voltage to VSI. 74LS07 and TLP250 are used as buffer and as gate driver respectively. The VSI uses Field programmable gate array (FPGA) Altera DE0 nano (cyclone IV) with QUARTES-II for its operation. The Fig. 15 (a) shows the block diagram and Fig. 15 (b) shows snapshot of prototype.

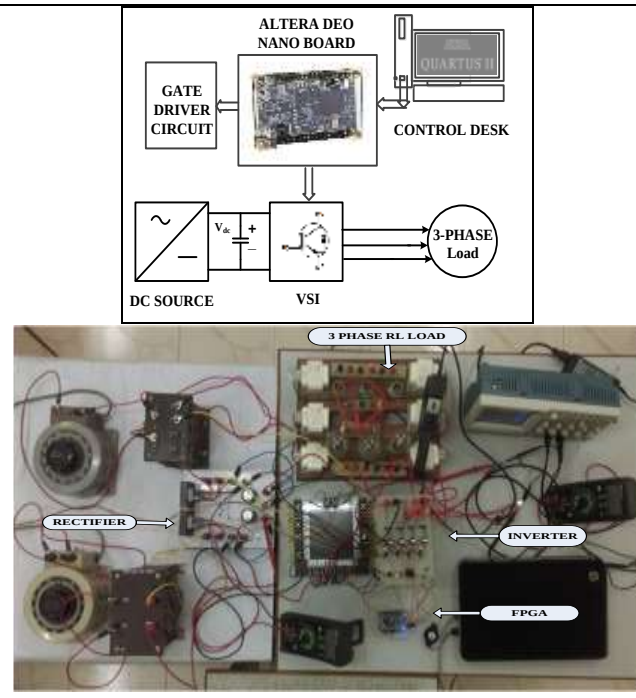

FIGURE 15. (a). Block diagram (b). Hardware prototype

Fig. 16 shows experimental results of 4 switching sequences of SVPWM i. e. conventional 0127, 30° clamped, 3 zone hybrid and 5 zone hybrid for VSI on a 2-kW R-L load at Unity MI. The 3 zone hybrid and 5 zone hybrid methods are presented in [31]. 30° bus clamping method is presented in [29]. The EDM sequence is taken as fifth candidate for comparison.

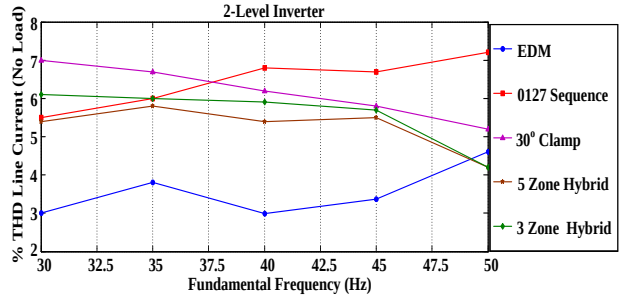

FIGURE 16. Measured line current %THD for various SVPWM methods for 50 Hz fundamental frequency at 2.44 kHz switching frequency for VSI.

It shows performance of EDM sequence is better than other sequences for different fundamental frequencies like 30 Hz, 35 Hz, 40 Hz and 45 Hz. For 50 Hz ripple of EDM sequence is only second to 3 zone hybrid method and 5 zone hybrid method. The sequence 0127 gives highest ripple among 6 sequences shown in Fig. 16 for 40 Hz, 45 Hz and 50 Hz.

The EDM method obtains mitigation in the line current THD for the range of 30 Hz to 50 Hz fundamental frequency for VSI by 81% as compared with the sequence 0127, by 40.7% as compared with the 30° Clamped method, by 27.5% as compared with the 5 Zone hybrid method and by 38.4% as compared with 3 Zone hybrid

ISSN PRINT 2319 1775 Online 2320 7876
 UGC CARE Listed (Group -I) Journal Volume 11, Iss 11, 2022

method. For two-level inverter over a range of 30 Hz to 50 Hz fundamental frequency.

Average % reduction in % current THD with EDM-SVPWM method as compared to any other technique 'X' can be calculated as follows;

Average % reduction in % Current THD by using EDM-SVPWM method as compared to any other method 'X' =

$$\left(\frac{\Sigma(\%\text{ current THD for method 'X'})-\Sigma(\%\text{ current THD for EDM})}{\Sigma\ (\%\ \text{CURRENT THD For Method X})}\right) * 100 \quad (28)$$

Results shown in Fig. 16 for line current THD are presented in tabulated form in Table V along with average % reduction values of other SVPWM techniques.

TABLE V
OBSERVATIONS FOR REDUCTION IN % CURRENT THD FOR EDM-SVPWM AND OTHER PROMINENT METHODS.

Sr No	f_1 Hz	% Current THD				
		EDM	0127	30° Clamped	5 Zone	3 Zone
1	30	3.01	5.5	7	5.4	6.1
2	35	3.81	6	6.7	5.8	6
3	40	2.99	6.8	6.2	5.4	5.9
4	45	3.37	6.7	5.8	5.5	5.7
5	50	4.61	7.2	5.2	4.2	4.2
Total (Σ)		**17.79**	**32.2**	**30.9**	**26.3**	**27.9**
Average % Reduction			**81.001**	**40.71**	**27.54**	**38.44**

Experimental result of line current and it's FFT spectrum for f_1 = 30 Hz, f_1 = 35 Hz, f_1 = 40 Hz, f_1 = 45 Hz and f_1 = 50 Hz for Unity MI are shown in Fig. 17, Fig. 18, Fig. 19, Fig. 20 & Fig. 21 respectively.

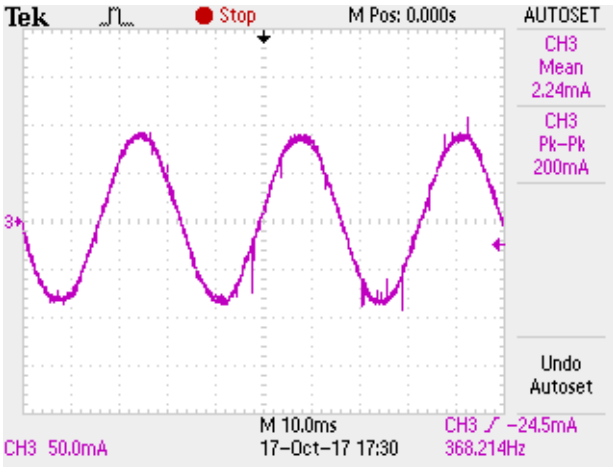

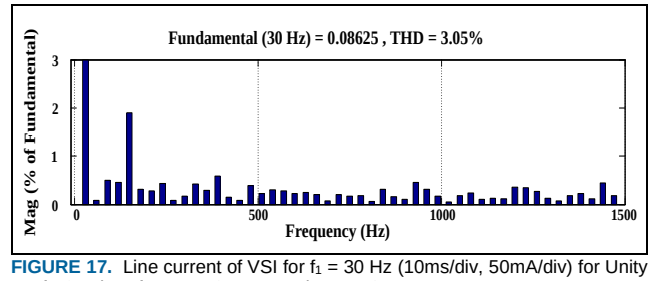

FIGURE 17. Line current of VSI for f_1 = 30 Hz (10ms/div, 50mA/div) for Unity MI, f_s=2.44kHz for EDM-SVPWM & its FFT Spectrum.

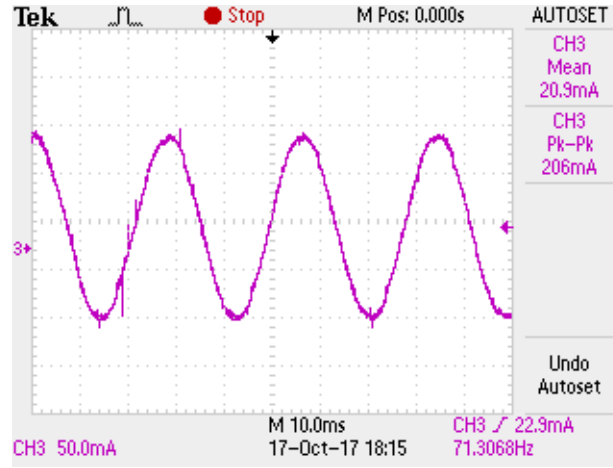

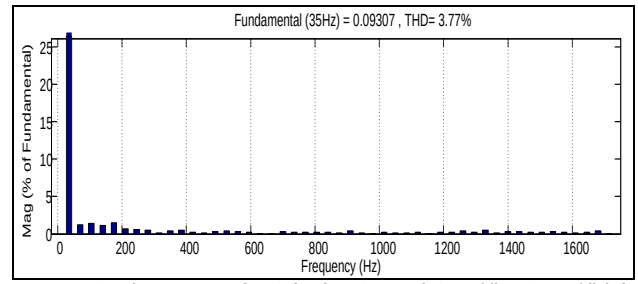

FIGURE 18. Line current of VSI for f_1 = 35 Hz (10 ms/div, 50 mA/div) for Unity MI, f_s = 2.44 kHz for EDM-SVPWM & its FFT Spectrum.

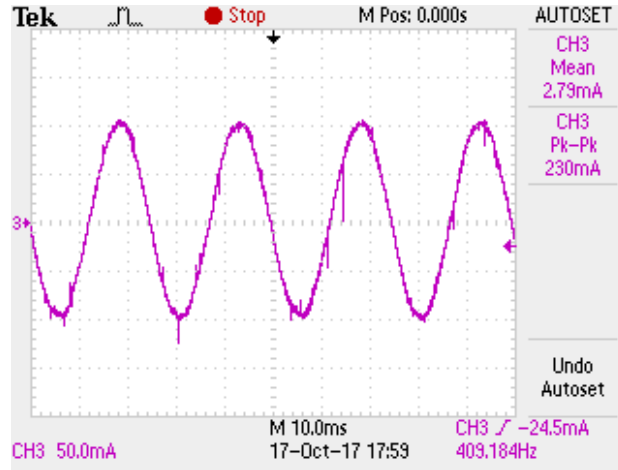

ISSN PRINT 2319 1775 Online 2320 7876
 UGC CARE Listed (Group -I) Journal Volume 11, Iss 11, 2022

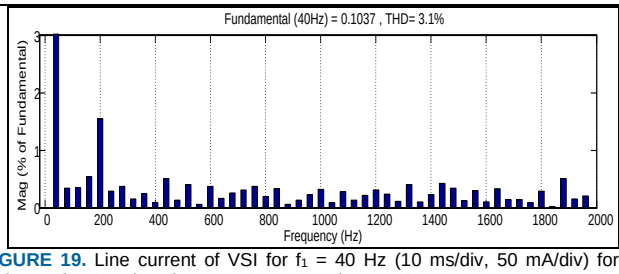

FIGURE 19. Line current of VSI for f_1 = 40 Hz (10 ms/div, 50 mA/div) for Unity MI, f_s = 2.44 kHz for EDM-SVPWM & its FFT Spectrum.

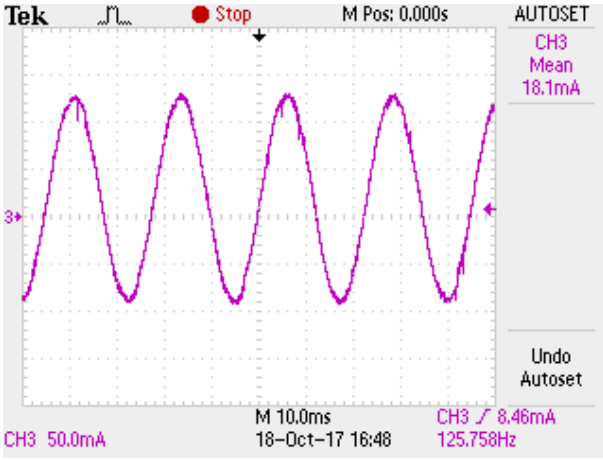

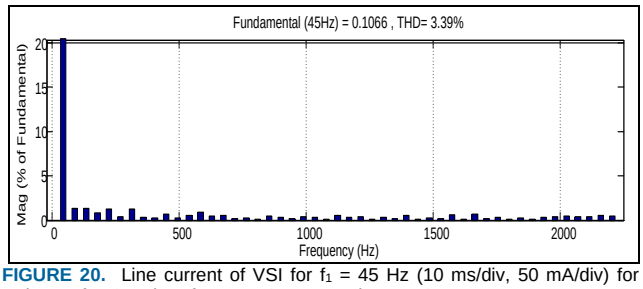

FIGURE 20. Line current of VSI for f_1 = 45 Hz (10 ms/div, 50 mA/div) for Unity MI, f_s = 2.44 kHz for EDM-SVPWM & its FFT Spectrum.

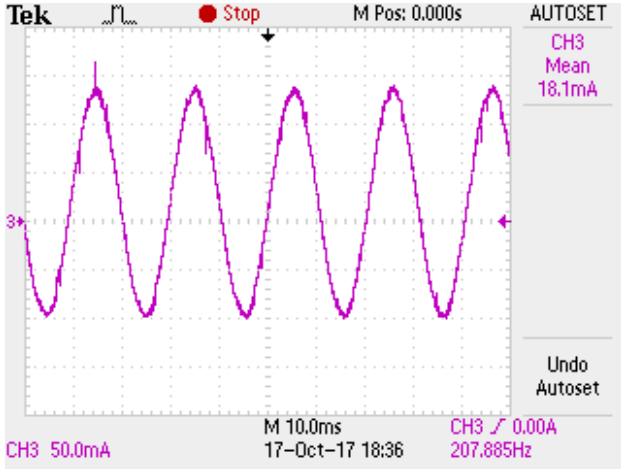

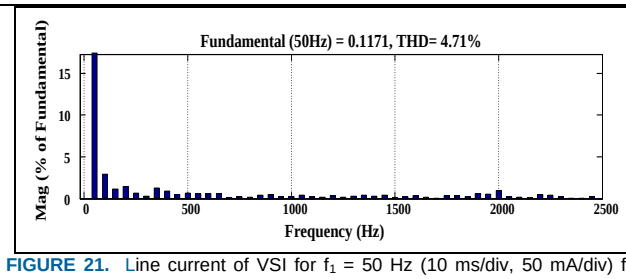

FIGURE 21. Line current of VSI for f_1 = 50 Hz (10 ms/div, 50 mA/div) for Unity MI, f_s = 2.44 kHz for EDM-SVPWM & its FFT Spectrum.

VII. CONCLUSION

The novel switching sequence design algorithm using EDM in SVPWM is presented in this manuscript. This algorithm simplifies implementation of SVPWM for VSI skipping complicated procedures needed in conventional SVPWM execution. Performance of proposed algorithm is tested in context of various critical parameters like mean square stator flux ripple 'F^2_{SEQ}', harmonic distortion factor 'F_{DIST}', harmonic contents in Voltage as well as in Line current of VSI. Out of the proposed EDM sequences, the 213 sequence gives the best performance. It achieves 7.35 % reduction in DF F_{Dist}, 5.5 % reduction in % voltage THD, 81.0% reduction in % line current THD as compared with 0127 sequence. The proposed technique also better than methods with respect to afore mentioned parameters. The unique concept of switching sequences based on ED calculations between V_{ref} and NTVs are proposed and their performances are compared with conventional and DSC switching sequences for variations in parameters like M.I., angle α° in a sector, fundamental frequencies and switching frequencies. These testing and comparison proves that proposed EDM-SVPWM technique and EDM switching sequences are worthy candidates. The hardware and analytical treatment results are provided to authenticate the performance EDM-SVPWM. Ease of execution with efficient performance is the most important virtue of the EDM-SVPWM Algorithm.

REFERENCES

[1] D. G. Holmes and T. A. Lipo, Pulse Width Modulation for Power Converters: Principles and Practice. Hoboken, NJ, USA: Wiley, 2003.

[2] A. M. Hava, R. J. Kerkman and T. A. Lipo, "Simple analytical and graphical methods for carrier-based PWM-VSI drives," *IEEE Transactions on Power Electronics*, vol. 14, no. 1, pp. 49-61, Jan. 1999.

[3] D. Casadei, G. Serra, A. Tani and L. Zarri, "Theoretical and experimental analysis for the RMS current ripple minimization in induction motor drives controlled by SVM technique," *IEEE Transactions on Industrial Electronics*, vol. 51, no. 5, pp. 1056-1065, Oct. 2004.

[4] G. Narayanan, D. Zhao, H. K. Krishnamurthy, R. Ayyanar and V. T. Ranganathan, "Space Vector Based Hybrid PWM Techniques for

Reduced Current Ripple," *IEEE Transactions on Industrial Electronics*, vol. 55, no. 4, pp. 1614-1627, April 2008.

[5] G. Narayanan, H. K. Krishnamurthy, D. Zhao and R. Ayyanar, "Advanced bus-clamping PWM techniques based on space vector approach," *IEEE Transactions on Power Electronics*, vol. 21, no. 4, pp. 974-984, July 2006.

[6] J. W. Kolar, H. Ertl and F. C. Zach, "Influence of the modulation method on the conduction and switching losses of a PWM converter system," *IEEE Transactions on Industry Applications*, vol. 27, no. 6, pp. 1063-1075, Nov.-Dec. 1991.

[7] D. Zhao, V. S. S. P. K. Hari, G. Narayanan and R. Ayyanar, "Space-Vector-Based Hybrid Pulsewidth Modulation Techniques for Reduced Harmonic Distortion and Switching Loss," *IEEE Transactions on Power Electronics*, vol. 25, no. 3, pp. 760-774, March 2010.

[8] Y. Wu, M. A. Shafi, A. M. Knight and R. A. McMahon, "Comparison of the Effects of Continuous and Discontinuous PWM Schemes on Power Losses of Voltage-Sourced Inverters for Induction Motor Drives," *IEEE Transactions on Power Electronics*, vol. 26, no. 1, pp. 182-191, Jan. 2011.

[9] K. Basu, J.S.S. Prasad, G. Narayanan.: 'Minimization of torque ripple in PWM AC drives', IEEE Trans. Ind. Electron., vol. 56, no. 2, pp. 553–558, Feb. 2009.

[10] K. Basu, J. S. S. Prasad, G. Narayanan, H. K. Krishnamurthy and R. Ayyanar, "Reduction of Torque Ripple in Induction Motor Drives Using an Advanced Hybrid PWM Technique," *IEEE Transactions on Industrial Electronics*, vol. 57, no. 6, pp. 2085-2091, June 2010.

[11] V. S. S. P. K. Hari and G. Narayanan, "Space-vector-based hybrid PWM technique to reduce peak-to-peak torque ripple in induction motor drives," IEEE Trans. Ind. Appl., vol. 52, no. 2, pp. 1489–1499, Mar./Apr. 2016.

[12] H. W. Van Der Broeck, H. C. Skudenly, and G. V. Stanke, "Analysis and realization of a pulsewidth modulator based on voltage space vectors," *IEEE Trans. Ind. Appl.*, vol. 24, no. 1, pp. 142–150, Jan./Feb. 1988.

[13] J. Rodríguez, J. S. Lai, and F. Z. Peng, "Multilevel inverters: A survey of topologies, controls and applications," *IEEE Trans. Ind. Electron.*, vol. 49, no. 4, pp. 724–738, Aug. 2002.

[14] A. K. Gupta, and A. M. Khambadkone, "A space vector PWM scheme for multilevel inverters based on two-level space vector PWM," *IEEE Trans. Ind. Electron.*, vol. 53, no. 5, pp. 1631-1639, Oct. 2006.

[15] J. H. Seo, C. H. Choi, and D. S. Hyun, "A new simplified space-vector PWM method for three-level inverters," *IEEE Trans. Power Electron.*, vol. 16, no. 4, pp. 545-550, Jul. 2001.

[16] N. Celanovic, D. Boroyevich, "A fast space vector modulation algorithm for multilevel three phase converters," *IEEE Trans. Ind. Appl.*, vol. 37, no. 2, pp. 637-641, Mar./Apr. 2001.

[17] Aneesh M.A.S., A. Gopinath, and M. R. Baiju, "A Simple Space Vector PWM Generation Scheme for Any General -Level Inverter," *IEEE Trans. Ind. Electron.*, vol. 56, no. 5, pp. 1649-1656, May 2009.

[18] A. Gopinath, Aneesh M. A. S., and M. R. Baiju, "Fractal Based Space Vector PWM for Multilevel Inverters—A Novel Approach," *IEEE Trans. Ind. Electron.*, vol. 56, no. 4, pp. 1230-1237, Apr. 2009.

[19] R. S. Kanchan, M. R. Baiju, K. K. Mohapatra, P. P. Ouseph, and K. Gopakumar, "Space vector PWM signal generation for multilevel inverters using only the sampled amplitudes of reference phase voltages," *Proc. Inst. Elect. Eng.*, vol. 152, no. 2, pp. 297–309, Mar. 2005.

[20] Irfan Ahmed; V. B. Borghate; A. Matsa; P. M. Meshram; H. M. Suryawanshi; M. A. Chaudhari, "Simplified Space Vector Modulation Techniques for Multilevel Inverters," *IEEE Trans. Power Electron*, vol. 31, no. 12, pp. 8483-8499, Dec. 2016.

[21] Y. Deng, Y. Wang, K. H. Teo, R. G. Harley, "A Simplified Space Vector Modulation Scheme for Multilevel Converters," *IEEE Trans. Power Electron*, vol. 31, no. 3, pp. 1873-1886, March 2016.

[22] A. Ovalle, M. E. Hernández and G. A. Ramos, "A Flexible Nonorthogonal-Reference-Frame-Based SVPWM Framework for Multilevel Inverters," *IEEE Transactions on Power Electronics*, vol. 32, no. 6, pp. 4925-4938, June 2017.

[23] B. S. Sakthisudhursun, J. Pandit, and M. Aware, "Simplified three level five-phase SVPWM," IEEE Trans. Power Electron., vol. 31, no. 3, pp. 2429–2436, Mar. 2016.

[24] T. Ishida, T. Miyamoto, T. Oota, K. Matsuse, K. Sasagawa and Lipei Huang, "A control strategy for a five-level double converter with adjustable DC link voltage," *Conference Record of the 2002 IEEE Industry Applications Conference. 37th IAS Annual Meeting (Cat. No.02CH37344)*, Pittsburgh, PA, USA, 2002, pp. 530-536 vol.1.

[25] J-H Youm and B. H. Kwon, "An effective software implementation of the space-vector modulation," IEEE Trans. Ind. Elctron vol.46, pp. 866-868, Aug. 1999,.

[26] S. Das and G. Narayanan, "Novel switching sequences for a space-vector modulated three-level inverter," *IEEE Trans. Ind. Electron.*, vol. 59, no. 3, pp. 1477–1487, Mar. 2012.

[27] S. Das, G. Narayanan, and M. Pandey, "Space-vector-based hybrid pulse width modulation techniques for a three-level inverter," IEEE Trans. Power Electron., vol. 29, no. 9, pp. 4580–4591, Apr. 2014.

[28] G. Narayanan and V. T. Ranganathan, "Analytical evaluation of harmonic distortion in PWM AC drives using the notion of stator flux ripple," *IEEE Trans. Power Electron.*, vol. 20, no. 2, pp. 466–474, Mar. 2005.

[29] G. Narayanan and V. T. Ranganathan, "Synchronised PWM strategies based on space vector approach. Part 1: Principles of waveform generation," *Proc. Inst. Elect. Eng.—Elect. Power Appl.*, vol. 146, no. 3, pp. 267–275, May 1999.

[30] G. Narayanan and V. T. Ranganathan, "Synchronised PWM strategies based on space vector approach. Part 1I : Performance assessment and application to V/f drives," *Proc. Inst. Elect. Eng.—Elect. Power Appl.*, vol. 146, no. 3, pp. 276–281, May 1999.

[31] V. S. S. P. K. Hari and G. Narayanan, "Space-vector-based hybrid pulse width modulation technique to reduce line current distortion in induction motor drives," *IET Trans. Power Electron.*, vol. 5, no. 8, pp. 1463–1471, Jul. 2012.

[32] M. Davies, M. Dommaschk, J. Dorn, J. Lang, D. Retzmann, and D. Soerangr, "HVDC PLUS - Basics and Principle of Operation." [Online]. Available: http://www.siemens.com/energy/hvdcplus.